Manufacturing method for high-amplitude corrugated thin-walled laminates

Composite Structures 222 (2019) 110925

Contents lists available at ScienceDirect

Composite Structures

journal homepage: www.elsevier.com/locate/compstruct

Manufacturing method for high-amplitude corrugated thin-walled laminates

D. Filipovic, G. Kress*

Laboratory of Composite Materials and Adaptive Structures, Department of Mechanical and Process Engineering, ETH Zürich, Tannenstr. 3, CH-8092 Zürich, Switzerland

ARTICLE INFO

Keywords:
Corrugated laminates
Composite materials
Manufacturing

ABSTRACT

Manufacturing of corrugated carbon-fiber reinforced composite laminates based on circular segments poses a challenge if high corrugation amplitudes create undercuts. This paper suggests to leave the formation of such high-amplitude corrugation shapes to thermal deformation of flat lay-ups which is effected by the difference between curing and service temperatures. It is shown by simulations that the method works best for carbon fibers of moderate stiffness and toughened epoxy-resin systems with high curing temperatures. Simple methods for predicting resulting shapes and stress distributions are explained and they verify non-linear structural simulations with FEM. A manufactured demonstrator validates the results. In addition to pointing out the new manufacturing method, some attention is paid to the potential application of corrugated laminates as flexible skins in morphing wings. It is pointed out how easily the morphing sections can be integrated into the manufacturing of wing skin and numerical stress analyses underline the strength feasibility of the manufacturing method. It comes as an additional benefit of the suggested manufacturing method that sliding overlaps can be integrated to create an aerodynamically smooth surface.

1. Introduction

Starting with the work of Yokozeki et al. [1], corrugated laminates made from fiber-reinforced materials are considered as candidate solutions for the flexible skins needed in morphing wing design, and receive much research attention [2,3]. Six of the ten papers on manufacturing methods mentioned in the literature review [3] allude in their titles to the application of corrugated laminates as flexible skins for morphing wings. This application for corrugated laminates is so obvious because of the extreme anisotropy along the corrugated direction and along the other direction transverse to it. The low inplane extensional stiffness along the corrugated direction provides for the desired compliance along the wing chord directions whereas the inplane extensional stiffness contributes via the parallel-axis theorem to the wing bending stiffness along the span direction, see Fig. 1 for illustration. Moreover, if the corrugation amplitude is very high, its extreme bending stiffness about the chord direction assigns the function of stringer to the corrugated laminate.

There are problems with the aerodynamic properties of corrugated laminates. One of those is that external pressure can lead to large deformations because of the high in-plane compliance along the chord and the bending compliance about the span directions. The structural response to uniform pressure of high-amplitude corrugated laminates with corrugation patterns consisting of circular sections has been studied by Thurnherr et al. [5] with the result that structural deflection is controlled by the extremely high bending stiffness about the chord direction and that the deflections can be kept very small if the corrugated laminate is supported by sliding rails at some sufficiently small spacing along the span direction. Airoldi et al. [3] report that the other aerodynamic problem is represented by the direct effects of corrugation on aerodynamic performance, and refer to the studies by Thill et al. [6] and Xia et al. [7]. It is stated in [3] that the studies elaborated a rule-of-thumb that the ratio of the height of corrugation to the chord length of the aerodynamic profiles must be kept at very low levels (<1%) to prevent a degradation of the performance.

1.1. Manufacturing methods for corrugated laminates

The patents by M.A. Chavannes and J.H. Lemelson [8,9] relate to the manufacture of corrugated materials for packaging purposes; these materials are not reinforced with fibers. W.R. Johnson and R.R. Welsh [10] patented a sine wave beam web and method of manufacture. The patent includes fiber-reinforced plastics and the manufacturing method requires molds. P.G. Donnecker et al. [11] disclose a method for making a corrugated fiber-reinforced preform for a corrugated channel. Their method requires shaping tools. A. Ashraf describes a method for producing a corrugated stretch laminate [12]. His method requires forming machinery.

* Corresponding author.
E-mail address: gkress@ethz.ch (G. Kress).

https://doi.org/10.1016/j.compstruct.2019.110925
Received 20 February 2019; Accepted 24 April 2019
Available online 30 April 2019

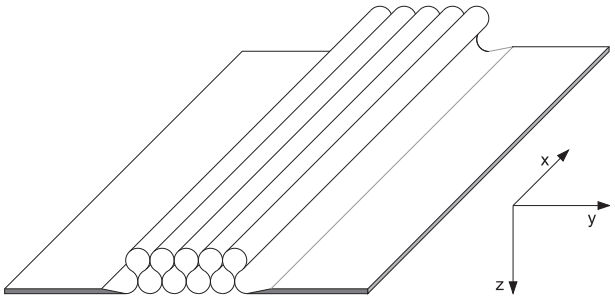

Fig. 1. Long plate with thin-walled corrugated section. Source [4].

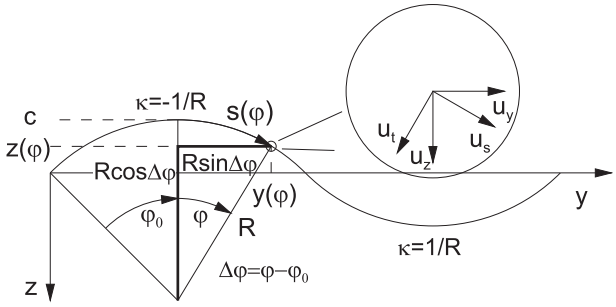

Fig. 2. Corrugated laminate reference coordinates. Source: [25].

Apart from applications as sandwich-core structures, the open literature considers corrugated laminates mostly in context of flexible skins for the application of morphing wings. Here, A. Airoldi et al. [3] provide a most recent literature review including manufacturing of corrugated laminates [1,13–19], where only Schmitz and Horst [19] consider corrugation shapes consisting of circular sections. Quality insurance in the production of thermoplastic sine wave beam production is addressed by Fischer et al. [20]. The circular-sections corrugation shape offers advantages regarding modeling ease [21,4] and distributions of interlaminar stresses [22].

Because of the undercuts appearing in high-amplitude circular-sections corrugation shapes, see Fig. 1, it is doubtful that mold-based manufacturing methods can be used for economic manufacturing processes. Forming with cylinders leaves the questions of how to obtain good laminate quality and how to arrive at reasonable manufacturing costs. The present authors believe that the only cost-effective method for creating such corrugated laminates are mold-less manufacturing methods such as suggested in the review paper by Khoo et al. [23] and more recently also addressed by Hoa [24]. The term mold-less refers to the circumstance that shells of a cylindrical shape can be formed by thermal curvature of unsymmetric flat laminates subject to temperature change, particularly the cool-down from curing to service temperatures.

1.2. Structure of the present paper

Performance prediction and preliminary sizing of corrugated laminates with circular-sections corrugation shape is possible with the relatively simple relations and formulas developed from the theories recalled in Section 2 *Mathematical background*. The question, whether realistic designs can be achieved with existing carbon-fiber reinforced thermoset plastics, is studied and answered in the affirmative in Section 3 *Feasibility study*. The steps for finding a practical design are summarized in Section 4 *Design procedure* and the principle of the manufacturing method, namely the layup pattern on a flat surface, is indicated in Section 5 *Manufacturing procedure*. Section 6 reports on the results of numerical simulations of the cooling process, thereby verifying the mathematical predictions by close agreement, and the analysis of the morphing behavior that eludes closed-form descriptions. This section confirms and extends the findings of the feasibility study in Section 3. The idea of adding sliding overlaps to the corrugated laminate is detailed in Section 7 *Aerodynamic sliding overlaps design* without further numerical simulations as those undertaken before remain valid; however, the lamination plan including the sliding overlaps is worked out and explained with Figs. 18–20. Plans for manufacturing a prototype demonstrator on a given rectangular plate of the size 2000 mm × 800 mm are laid out in Section 8 *Demonstrator*. Remaining problems and their potential mitigations are addressed in Section 9 *discussion* and the conclusions are found in Section 10.

2. Mathematical background

The theoretical background for predicting corrugated shapes includes the classical theory of laminated plates and some geometric description of corrugation shapes consisting of circular sections.

2.1. Circular-sections corrugation shape geometry

Fig. 2 indicates the reference coordinates in which the corrugated laminate is described and the curvilinear coordinates along the laminated sheet mid-plane. The relation between circular-segments radius R, corrugation amplitude c, and periodic length of the corrugation pattern P is given with [21]:

$$R = \frac{16c^2 + P^2}{32c}. \tag{1}$$

This equation is rearranged to calculate the periodic length of one corrugation-pattern unit cell for given reference-shape curvature R and the ratio $\bar{c}$ that is the corrugation amplitude c normalized with respect to the periodic length P:

$$P = R\frac{32\bar{c}}{16\bar{c}^2 + 1}; \quad \bar{c} = \frac{c}{P}, \tag{2}$$

where Fig. 3 illustrates that the normalized amplitude $\bar{c}$ is a shape characteristic. The condition that the corrugated laminate with sheet thickness t must not penetrate itself gives the upper bound of the corrugation amplitude c [25]:

$$0 \leqslant c \leqslant \frac{P - t + \sqrt{(P-t)^2 - \frac{P^2}{4}}}{2}. \tag{3}$$

The curved-sheet length L_s, covering one period of corrugation, is given with [21]:

$$L_s = 4\psi_0 R, \tag{4}$$

where the opening angle ψ_0 is defined in Fig. 2 and is calculated by [4]

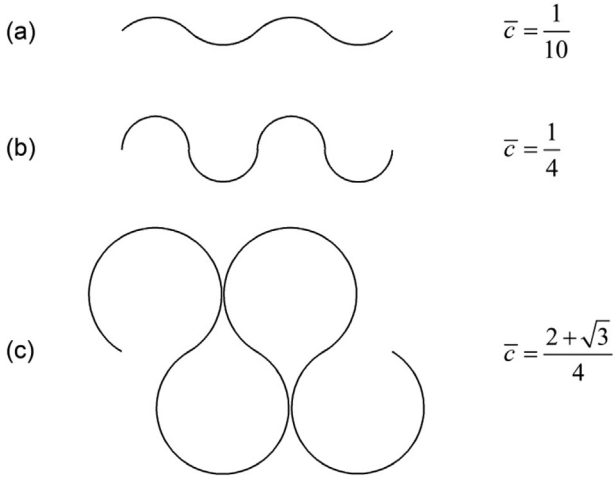

Fig. 3. Shapes and amplitude-periodic-length ratios. Source: [21].

$$\psi_0 = acos\left(1 - \frac{c}{R}\right). \tag{5}$$

2.2. Excerpts of the classical theory of laminated plates

The proposed manufacturing method relies on temperature-induced curvature where the ratio of laminate thickness t to bending radius R remains rather small so that the classical theory of laminated plates (CTLP) [26] is applicable. The circular-section radius R is estimated by the bending curvature suffered by an unsymmetric laminate due to an apparent temperature difference ΔT between curing and service temperatures. The deformations of an infinitesimally small plate element under mechanical and thermal loads are calculated with

$$\begin{Bmatrix}\mathbf{N}\\ \mathbf{M}\end{Bmatrix}^{equ} + \begin{Bmatrix}\mathbf{N}\\ \mathbf{M}\end{Bmatrix}^{mec} = \begin{bmatrix}\mathbf{A} & \mathbf{B}\\ \mathbf{B} & \mathbf{D}\end{bmatrix}\begin{Bmatrix}\boldsymbol{\varepsilon}^0\\ \boldsymbol{\kappa}\end{Bmatrix}, \tag{6}$$

where the superscripts ^{equ} and ^{mec} indicate line loads equivalent to thermal loading and mechanical line loads; respectively, and where the equivalent line loads are calculated by

$$\begin{Bmatrix}\mathbf{N}\\ \mathbf{M}\end{Bmatrix}^{equ} = \sum_{k=1}^{N} \bar{\mathbf{Q}}_k \bar{\boldsymbol{\alpha}}_k \begin{Bmatrix}(z_k - z_{k-1})\\ \frac{1}{2}(z_k^2 - z_{k-1}^2)\end{Bmatrix}\Delta T. \tag{7}$$

where $\bar{\mathbf{Q}}_k$ and $\bar{\boldsymbol{\alpha}}_k$ are reduced stiffness matrix and coefficients of thermal expansion; respectively, transformed to the reference system. These equations calculate double curvatures corresponding with saddle shapes of plates of moderate extension [27]. Corrugated laminates, on the other hand, correspond with cylindrical bending,

$$\kappa_{xx} \approx 0, \tag{8}$$

where the direction x is indicated in Fig. 1, if the corrugation amplitudes are sufficiently large with respect to periodic length but much smaller than the extension transverse to the corrugations. The following mechanical line forces must vanish:

$$N_x = N_{xy} = M_{xy} = 0. \tag{9}$$

The line shear force N_{xy} and the line torsional moment M_{xy} vanish for cross-ply laminates if no shear deformation or twist are applied. Obeying these constraints coming from cylindrical bending gives a more accurate estimate of the temperature deformations under cylindrical bending with the following equations to be resolved for the mid-plane strains and the curvature:

$$\begin{Bmatrix}N_x\\ N_y\\ M_y\end{Bmatrix}^{fict} = \begin{bmatrix}A_{11} & A_{12} & B_{12}\\ A_{12} & A_{22} & B_{22}\\ B_{12} & B_{22} & D_{22}\end{bmatrix}\begin{Bmatrix}\varepsilon_x^0\\ \varepsilon_y^0\\ \kappa_y\end{Bmatrix}. \tag{10}$$

where the equivalent and the mechanical line loads in (6) combine to give the fictitious line loads indicated with superscript ^{fict}. The laminate total-strain distributions are given with:

$$\boldsymbol{\varepsilon}(z) = \boldsymbol{\varepsilon}^0 + z\boldsymbol{\kappa} = \begin{Bmatrix}\varepsilon_x^0\\ \varepsilon_y^0\\ 0\end{Bmatrix} + z\begin{Bmatrix}0\\ \kappa_y\\ 0\end{Bmatrix}. \tag{11}$$

Stresses in laminate layer k are calculated with

$$\boldsymbol{\sigma} = \bar{\mathbf{Q}}_k[\boldsymbol{\varepsilon}(z) - \boldsymbol{\alpha}_k \Delta T] \tag{12}$$

In the absence of mechanical loads, the local stresses in (12) are referred to as residual stresses. They arise with change of temperature away from a stress-free reference temperature. In the curing process of composite materials with thermo-set matrices, the curing temperature is estimated to be stress-free. Moreover, the coefficients of thermal expansion (CTE) are assumed to remain constant between curing and service temperatures. For strength prediction the local stresses have to be transformed into material coordinates.

Table 1
Relevant material properties of unidirectional composites with fiber-volume fraction $v_f = 0.6$. Source: DORNIER SYSTEM GmbH.

Fiber	E_1	E_2	ν_{12}	α_1	α_2
	[MPa]		[–]	[10^{-6}/K]	
T 300	135000	10000	0.27	− 0.6	30
M 40	220000	7000	0.35	− 0.8	30
GY 70	290000	5000	0.41	− 1.0	30

3. Feasibility study

The feasibility study addresses the questions:

1. is it possible to achieve sufficiently high thermal curvature with realistic laminate thickness?
2. will the residual stresses remain small enough to guarantee strength?
3. will the margins of strength be large enough to allow for sufficient morphing deformations?

3.1. Materials and coefficients of thermal curvature

The feasibility study considers three typical carbon-fiber reinforced epoxies where Table 1 shows the relevant material properties of prepregs with layer thickness $h = 0.125$ mm. The aforementioned situation of cylindrical bending gives, upon resolving (10) for the plate deformations and then dividing these by the temperature change ΔT, the thermal curvature coefficients that are listed in Table 2. The same numbers are marked with the open symbols in Fig. 4. The other values marked with solid symbols are calculated under the assumption that the laminate properties are only considered locally (infinitesimal small plate element) where no constraints apply. It can be seen that the constraint of cylindrical bending has a relatively small influence on the coefficients of thermal curvature (CTC). All materials find higher CTC values for numbers n_0, of span-wise oriented layers, larger than one. $T300$ and $M40$ find the highest values for $n_0 = 2$ and $GY\ 70$ for $n_0 = 3$. The highest CTC values are obtained by $T300$ which we ascribe to the relatively small Young's modulus in fiber direction that allows higher bending. We conclude that, out of the present selection, laminates [90/0] or [90/0_2] made from $T300$ epoxy prepreg are best candidates for making corrugated laminates with the help of thermal deformation.

We assume that $\Delta T = -150$ °C is a realistic temperature difference available for creating curvature for thermoset resin types with curing temperature of $T_{cur} = 180$ °C. It will create a bent-shape radius of

$$R = \frac{1}{\kappa_y^T \Delta T} \tag{13}$$

For the laminates [90/0] and [90/0_2] we find $R = 65.1$ mm and $R = 61.4$ mm, respectively. The corresponding ratios between thickness and radius of 196.4 and 123.3; respectively, are visualized with the true-scale sketches in Fig. 5

3.2. Laminate thermal deformation coefficients

Laminate symmetry prevents thermal curvatures to appear, see the

Table 2
Temperature-curvature coefficients κ_y^T [10^{-4}/mm K].

Fiber	[90/0]	[90/0_2]	[90/0_3]	[90/0_4]
T 300	1.0233	1.0863	0.8863	0.7149
M 40	0.6348	0.9081	0.8395	0.7148
GY 70	0.4066	0.7214	0.7571	0.6848

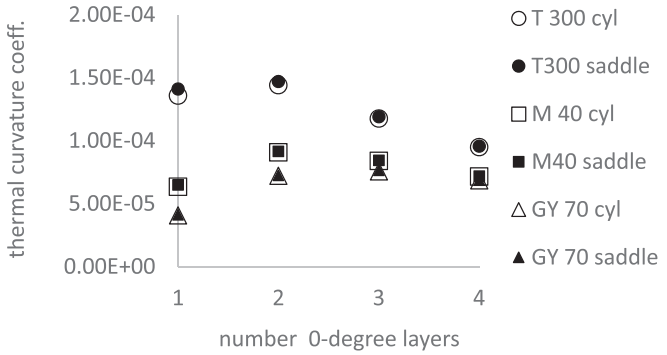

Fig. 4. Thermal curvature coefficients for cylindrical bending (open markers) and for unconstrained infinitesimal small plates (solid markers).

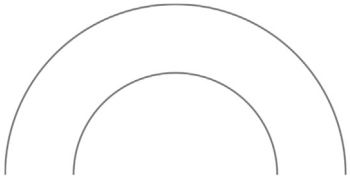

Fig. 5. R/t ratios 260 and 164 drawn to scale for unit wall-thickness.

Table 3
Laminate thermal-deformation coefficients (T300).

	$[90/0_2]_s$	$[90/0_2]$ saddle	$[90/0_2]$ cylinder
ε_x^0 [10^{-6}/K]	3.800	2.47	− 0.638
ε_y^0 [10^{-6}/K]	0.956	14.90	14.767
κ_x [10^{-6}/mm/K]	0.000	− 32.80	0.000
κ_y [10^{-6}/mm/K]	0.000	110.00	108.630

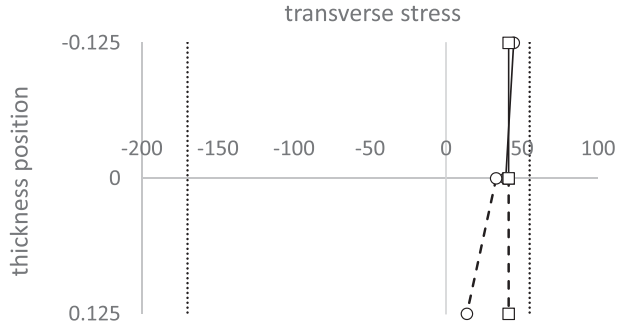

Fig. 6. σ_2 in [90, 0] laminate, solid lines in 90° layer, dashed lines in 0° layer, vertical lines correspond with total bending constraint, dotted lines indicate material strength.

left column in Table 3. A typical laminate-analysis program assumes no deformation constraints under line loads so that for an unsymmetric laminate both curvature components appear, see the center column in the table. Cylindrical bending implies that one of the two bending curvatures must be zero. This constraint changes the laminate deformation coefficients as can be seen in the right column of the table; however, midplane strain ε_y^0 and the non-vanishing curvature κ_y differ only slightly from those of the unconstrained laminate. However, the relatively large change of ε_x^0 might affect residual stresses significantly. (See Figs. 6 and 7).

3.3. Residual stresses

It has been seen that the residual stresses in fiber direction, σ_1, are always so much less than the respective stress limits that fiber failure is not an issue. Therefore, Tables 4 and 5 list residual stresses transverse to the fiber direction, σ_2, for the symmetric and the unsymmetric laminates [90/0] and [90/0_2]; respectively. The symmetric versions are free of bending and the unsymmetric versions are subject to temperature load without any kinematic constraint (saddle) and the cylindrical-bending constraint (cylinder). The material strength is assessed with the margin of safety

$$M_S = \frac{X_t - \sigma_2}{\sigma_2} \tag{14}$$

For the symmetric [90/0] laminate, the transverse stresses are tensile and the same in all layers, giving a uniform margin of safety of $M_S = 33\%$ for the material with transverse tensile strength $Y_t = 55$ MPa. The same stresses are much smaller in the unconstrained laminate whereas the constraint of cylindrical bending about the x direction reduces the stress in the 0° layer significantly but the maximum stress in the 90° is slightly increased, reducing the margin of safety down to $M_S = 24\%$. For the symmetric [90/0_2] laminate the transverse stresses are tensile but slightly higher in the 90° ($M_S = 31\%$) than in the 0° layers. The constraint of cylindrical bending about the x direction reduces the stress in the 0° layer significantly but the maximum stress in the 90° direction is increased, reducing the margin of safety down to $M_S = 19\%$. Transverse stresses at the surface $z = 0.1875$ become compressive but do not challenge the strength of $Y_c = 170$ MPa. Figs. 6 and 7 give a visual impression of the stress distributions based on the data provided in the tables. Stresses within the 90° and 0° are plotted with solid and dashed lines, respectively. The vertical lines marked with

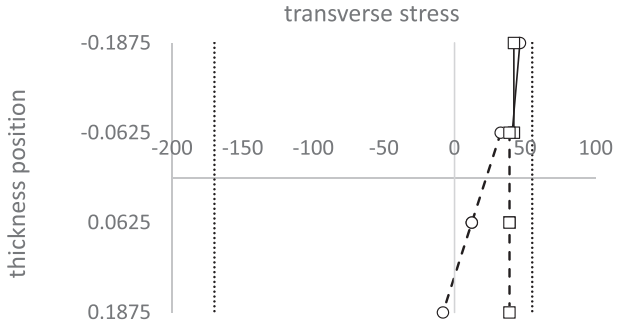

Fig. 7. σ_2 in [90, 0_2] laminate, solid lines in 90° layer, dashed lines in 0° layers, vertical lines correspond with total bending constraint, dotted lines indicate material strength.

Table 4
Stresses σ_2 [*MPa*] at ply interfaces (IF) in laminate [90/0].

ply	deg	IF	$[90/0]_s$	[90/0] saddle	[90/0] cylinder
1	90	bot	41.2	16.0	44.5
1	90	top	41.2	30.6	39.3
2	0	bot	41.2	30.6	33.0
2	0	top	41.2	16.0	13.7

Table 5
Stresses σ_2 [*MPa*] at ply interfaces (IF) in laminate [90/0_2].

ply	deg	IF	$[90/0_2]_s$	$[90/0_2]$ saddle	$[90/0_2]$ cylinder
1	90	bot	42.0	34.4	46.3
1	90	top	42.0	34.9	40.8
2	0	bot	38.9	31.2	32.7
2	0	top	38.9	12.0	12.2
3	0	bot	38.9	12.0	12.2
3	0	top	38.9	− 7.1	− 8.2

open squares give the stress distributions without bending deformation as they occur in symmetric laminates. The slanted lines marked with open circles correspond to cylindrical bending. Dotted lines indicate the tensile-stress and compressive-stress limits, respectively. Morphing action applied to maximum-amplitude corrugated laminates will tend to reduce the thermally induced bending curvature so that the stress distributions will move closer to those of the symmetric laminates, thereby reducing the highest tensile stresses. The analysis of residual stresses indicates feasibility of the proposed manufacturing method.

3.4. Increasing margins of safety

Even though the residual-stress analysis indicates feasibility, an increase of the static margins of safety is desirable with hindsight to often-repeated morphing action, or fatigue loading.

One of the measures is to choose a material with higher transverse tensile strength Y_t than the ones considered in here (either strongly toughened epoxy matrix systems or thermoplastics with curing or melting temperatures; respectively, around $T = 180\,°C$). The other measure is to use a lower process temperature, say $T = 120\,°C$. This would give a lower effective temperature change and, consequently, lower residual stresses. The disadvantage of having a lower thermal curvature can be mitigated by accepting a corrugated shape with lower amplitude, see sketch to the left in Fig. 11, which could then be compressed by mechanical actuation so that the high-amplitude shape shown with the center plot in the same figure results.

4. Design procedure

The structural requirement of a given application may lead to other laminate designs as suggested in the feasibility study. The design procedure described in here focuses on finding the information for making the lay-up in terms of prepreg patches for a desired corrugated shape. It includes finding a shape for reduced stressing under applied global strain in the corrugated direction.

1. obtain material data and curing process data
2. specify unsymmetric laminate design
3. calculate temperature curvature → shape radius R
4. choose c/P ratio for desired shape
5. calculate periodic length P
6. perform stress analysis
7. calculate curved length L_s for cutting prepreg

Step 3 requires application of the classical theory of laminated plates. Steps 4 through 6 may be iterated for maximizing the margin of safety against inter-fiber failure (matrix failure or debonding). Step 5 requires (2).

5. Manufacturing procedure

Fig. 8 indicates a schematic of the design principle integrating flat and corrugated sections in one manufacturing process. The section, assuming a corrugated shape by to cooling after curing, is within the dashed vertical lines. Outside of this section, the laminate increases gradually in thickness where the figure suggests simple tapering. Interlaminar shearing or peeling stresses in the tapering will be very small as only small line loads can be transmitted along the corrugated direction. A 90-degree layer runs throughout the corrugated part in order

Fig. 8. Stacking sequence for one complete corrugation period. Dashed lines indicate transition to non-morphing parts of the design. For better visualization, the ratio between length and thickness is not to scale.

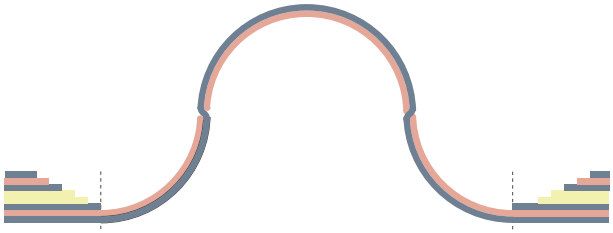

Fig. 9. Laminate after manufacturing process. Shown semi-circle shape aerodynamically bad.

to avoid lap jointing. The lay-up ensues from bottom to top on a flat substrate (or a shallow-curved substrate for the aerodynamic shape of a wing). After lay-up, the standard steps of vacuum bagging and curing in an autoclave must be performed to obtain the formed design shown in Fig. 9.

The advantages of the suggested manufacturing method include:

1. no tooling other than for flat laminates required
2. same high quality as of flat laminates
3. additional manufacturing effort marginal
4. fully integrated design of corrugated parts in skin
5. automation potential: automated tape laying
6. →extremely low cost for realizing morphing wing

6. Numerical process simulations

The geometrically nonlinear structural analysis with the finite-element method (FEM) simulates the creation of corrugation patterns by thermal deformation due to cooling after curing. The post-processing obtains stress distributions through the thickness.

6.1. Simulation tools

A FORTRAN data generator reads the data from the text file shown in Fig. 10. It then generates a text file containing *ANSYS Parametric Design Language* (APDL) commands for controlling the steps of the structural analysis. The bending-radius estimate R must be obtained by the classical theory of laminates plates and be in agreement with the specified temperature drop ΔT. With the information of the curves length, obtained from the other input data, areas are created for each corrugation-pattern unit cell according to the scheme indicated with the region in between the dotted lines in Fig. 8. The areas are then attributed the respective material laws for 90° and 0° layers. Mesh density is determined by using one row of square finite elements per layer so that

```
LAYER THICKNESS                          H :          0.1250
NUMBER OF ZERO-DEGREE LAYERS           N_0 :               1
AMPLITUDE TO PERIODIC LENGTH        C_TO_P :           0.933
BENDING RADIUS ESTIMATE                  R :            65.1
NUMBER OF PERIODS                      N_P :               1
TEMPERATURE CHANGE                 DELTA_T :          -150.0
# TEMPERATURE LOAD STEPS      N_STEPS_TEMP :              30
APPLIED GLOBAL STRAIN [%]            EPS_Y :             0.0
# STRAIN LOAD STEPS           N_STEPS_EPS :               0
-------------------------------------------------------------
CURVED LENGTH                          S_L :          681.7
```

Fig. 10. Data generator text input file.

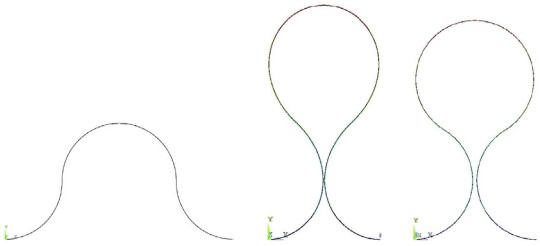

Fig. 11. Corrugated semi-circular shape obtained by thermal load $\Delta T = -150$ °C.

the mesh comprises a total of 10,910 planar elements for the data shown in Fig. 10. The elements (ANSYS PLANE183) have quadratic shape functions so that mapping of linear bending-strain distributions is within the element-type solutions space.

6.2. Deformed shapes

Fig. 11 contains plots of deformed corrugation shapes of one unit cell. The plot to the left shows that the FEM simulation reproduces quite closely the intended semi-circular shape due to thermal loading. Compressing this corrugated laminate by a line force produces the shape shown with the center plot. The mechanical deformation naturally causes shape deviations away from circular sections. A maximum-amplitude shape, caused by thermal deformation alone, is shown in the plot to the right.

6.3. FEM residual stress evaluations

The color coding in Fig. 12 depicts the distribution of the stress σ_x within a small section of the 0° layer at the apex of the corrugation pattern shown with the plot to the right in Fig. 11. It can be taken from the false-color scaling shown in Fig. 12 that minimum and maximum stress values (13.5/33) agree closely with those values obtained by the classical theory of laminates plates under the constraint of cylindrical bending listed in Table 4 (13.7/33).

Next we show that residual stresses can be reduced by the process indicated with the leftmost and center plot in Fig. 11, where the resulting stresses are evaluated with FEM simulations and shown in Table 6. Because of the planar plane-stress finite elements only the transverse stresses in the 0° layers can be calculated. The columns in the table correspond with the respective plots in Fig. 11. It can be seen that the lowering the curing temperature decreases the residual stresses proportional to the decrease in temperature change. Subsequent enforcing the displacement for obtaining a maximum-amplitude shape reduces the stresses to the values shown in the center column of the table.

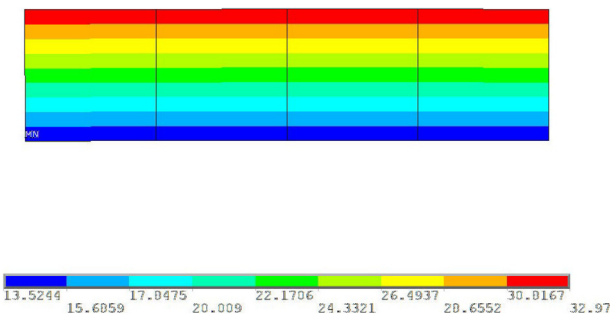

Fig. 12. FEM evaluation of σ_x within 0° layer at corrugation apex.

Table 6
Stresses σ_2 [MPa] and margins of safety at ply interfaces in laminate [90/0] according to different process routes.

ΔT [°C]	− 80	− 80.0	− 1.0
$\hat{u}_x$ [mm]	0	− 16.3	0
Bot	7.5	− 8.60	13.5
Top	18.2	13.7	33.0
M_S [%]	200	301	67

Table 7
Geometries for laminate [90/0], $\Delta T = -150$ °C.

Version	$\frac{c}{P}$	R	L_S	P
Maximum amplitude	0.933	65.1	681.7	130.2
Semi circles	0.25	65.1	409.0	260.4

6.4. Morphing behavior

We consider, for the laminate [90/0], the morphing ranges of the two manufacturing versions indicated in Fig. 11. Key geometric data obtained by the theories outlined in Sections 2.1 and 2.1 and needed as input for the FEM simulations are listed in Table 7. The stresses presented in the diagrams in Figs. 14 and 16 have been read out at the corrugation apexes, which will first reach an unbent shape as can be seen in Fig. 13 that shows a plot of the initially semi-circular corrugation at the end of the morphing action. We obtain virtually identical results with a recent analytical nonlinear morphing model [28]; however, the results of it are not presented here because the present work and the new model have been developed in parallel.

6.4.1. Maximum-amplitude shape

Within the morphing range mapped in Fig. 14, the stresses at both interfaces of the 0° layer increase linearly with morphing strain. At the intersection of the linear approximations the stress at both interfaces are equal, indicating complete unbending. Assuming that the stress diagrams remain linear up to the intersection point, estimates the morphing-strain capacity at $\varepsilon_{morph} \approx 76\%$.

The morphing line force shown in Fig. 15 increases progressively with the morphing strain; however, the values remain quite small, $N_y \leqslant 0.0035$ N/mm. At full extension of the corrugated laminate, shown with Fig. 13, and for a structure of a length of 10 m, the total actuation or reaction force, respectively, amounts to only 35 N.

6.4.2. Semi-circular shape

The origin of the strain axis in the plots, shown in Figs. 14 and 17, corresponds with the manufactured semi-circular which needs to be compressed to approximate a maximum-amplitude shape where the morphing strain has the value of $\varepsilon_{morph} = -44\%$. Fig. 16 reveals that the stresses do actually not continue to increase linearly up to the intersection point as perfect unbending will not occur before the local line becomes more dominant than the bending moment at the apex. Nevertheless, the diagrams run over a morphing strain range of $\varepsilon_{morph} = 75\%$.

Fig. 17 shows that the reacting morphing line force increases strongly non-linear with increasing strain [22]; however, due to the large ratio of radius to laminate thickness the force remains very small $N_y = 0.018$ N/mm.

Fig. 13. Semi-circular corrugation at the limit of morphing action.

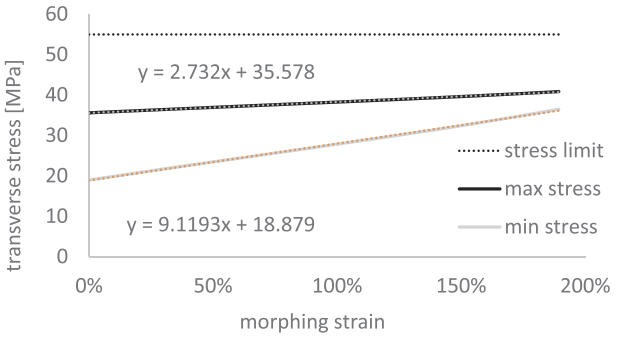

Fig. 14. Apex stresses σ_2 versus morphing strain for $\frac{c}{P} = 0.933$.

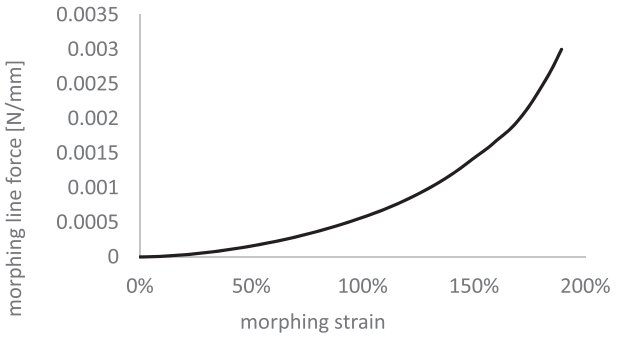

Fig. 15. Line force N_y versus morphing strain for $\frac{c}{P} = 0.933$.

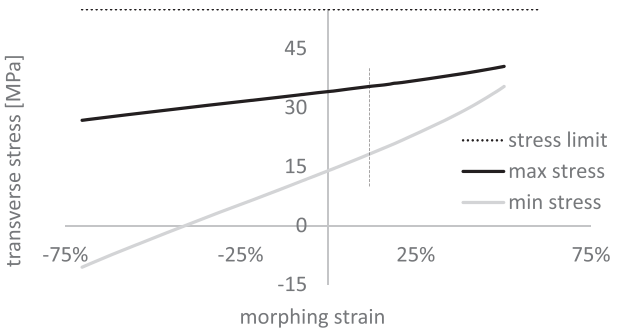

Fig. 16. Apex stresses σ_2 versus morphing strain for $\frac{c}{P} = 0.25$.

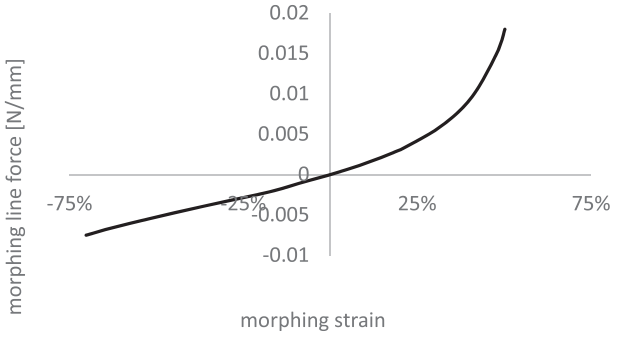

Fig. 17. Line force N_y versus morphing strain for $\frac{c}{P} = 0.25$.

6.4.3. Versions comparison and discussion

That the semi-circular shaped corrugations allow for a higher morphing-strain capacity (75%) than the maximum-amplitude shape (55%), is explained by the fact that, in compressed state where its shape is similar to the maximum-amplitude shape, a higher curvature appears at the apexes so that, from that position on, a greater extension is needed to achieve almost perfect unbending. In that almost unbent deformation the maximum transverse stresses for both shapes must be nearly the same. At both 0°-layer interfaces, the change of stresses during morphing action is significantly greater for the semi-circular shape than for the maximum-amplitude shape. Even though we do not intend to perform a fatigue-behavior study at this point, we would like to point out that inter-fiber failure in the 0°-layer will release residual stresses which maintain the circular shape. (Table 8)

Table 8
Comparison of versions.

Version	$\Delta\varepsilon_{morph}$ [%]	σ_{max} [MPa]	$\Delta\sigma_{bot}$ [MPa]	$\Delta\sigma_{top}$ [MPa]
Semi circles full ext	204	41	46	14
Maximum amplitude	189	41	18	5

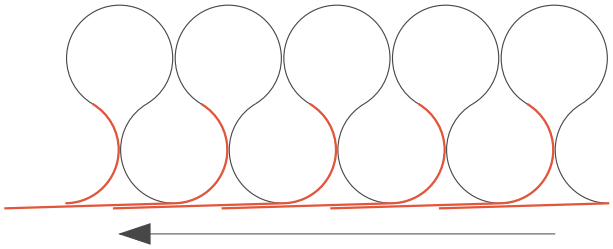

Fig. 18. Aerodynamic scales design; arrow indicates air flow direction.

7. Aerodynamic sliding overlaps design

The new fabrication method solves the much lamented problem of the aerodynamic penalty of corrugated flexible skins: Fig. 18 shows that parts of the laminate can be designed so that they serve as sliding overlaps covering the corrugations and creating a closed aerodynamically smooth surface. The sliding overlaps must be long enough to cover the corrugations over the entire morphing range of about 55%. They tend to be closed by a higher air pressure dominating at the bottom of the profile. As the overlaps cannot pick up the elastic energy necessary to support self exciting vibrations, flutter cannot occur. The sliding overlaps are laminated together with the other layers along the curved sections as indicated in Fig. 18. In order to not work against the thermal curvature, they must be of the same fiber orientation as the adjacent 90° layer. This implies high stiffness and strength of the sliding overlaps along the chord direction so they do not break off easily. On the other hand, they do not contribute much to span-direction stiffness. As the overlaps, or scales, contribute to 90° layer thickness, the lamination plan shown in Fig. 20 foresees double numbers of the respective layers. To maintain similar thermal curvature coefficients as listed in Table 2, and with them similar geometric corrugation parameters, individual layers must be of half the thickness as considered in previous sections, namely 0.125 mm → 0.0625 mm, where the smaller thickness is realistic as such prepregs are commercially available.

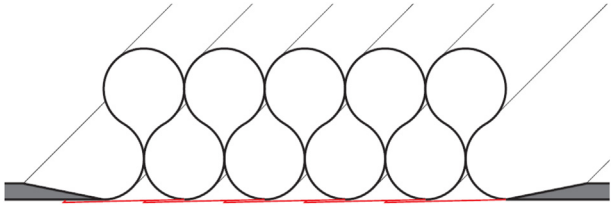

Fig. 19. Detail of long plate with thin-walled corrugated section and integrated sliding overlaps (red). (For interpretation of the references to colour in this figure legend, the reader is referred to the web version of this article.)

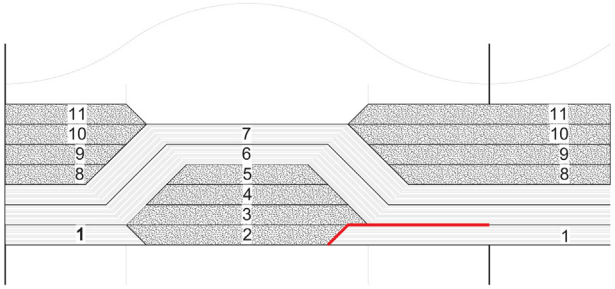

Fig. 20. Scales design lamination scheme. Length-to-thickness ratios not realistic. Red line indicates separation of scale from the rest of the laminate by Teflon foil. (For interpretation of the references to colour in this figure legend, the reader is referred to the web version of this article.)

8. Demonstrator

8.1. Autoclave size

Of the plate area of 800 mm × 2000 mm some edge width must be foreseen for applying the sealing material for the vacuum bagging. We choose a net lay-up area of 700 mm × 1900 mm. Because of the large curved lengths of one period of a maximum-amplitude shape of 680 mm it must be that the corrugations are placed along the longer plate extension.

8.2. Material

A prepreg made by *North Thin-Ply Technologies*, namely NTPT THINPREG™ 513, was used to make demonstrator prototypes as it was already available at our lab. Table 9 lists values found in available data sheets for fiber and matrix whereas the composite properties have been estimated with the simplified equations by Chamis [29].

8.3. Prototype for measuring thermal curvature

The first prototype-laminate consists of three regions,
$[90/0_2] - [0_2/90] - [90/0_2]$, where the outer regions measure 50 mm along the 0° direction and the inner one 100 mm. The dimension of the laminated plate along the other direction is 100 mm. The outer regions with reversed stack-up sequence help to suppress saddle shapes. We used a processing temperature of $T_{proc} = 120$ °C. Fig. 21 shows he resulting part after applying the autoclave process. The thickness of a 3-layer laminate was measured at 0.18 mm so that cured layer thickness is 0.06 mm. At a room temperature of about 20 °C, its radius of curvature has been measured as $R = 35.7$ mm. Using the material properties listed in Table 9, we predicted the curvature radii shown in Fig. 22 which shows good agreement, particularly for the higher temperature difference $\Delta T = -100$ K.

Table 9
Material properties. Young's moduli [MPa], CTE [10^{-6} K^{-1}].

Fiber T800	E_{fL} 29400	E_{fT} 1600	α_{fL} − 0.3	α_{fT} 28.1	ν_{fL} 0.2	ν_{fT} 0.01
Matrix 513	E 4100		α 55.0		ν 0.3	
Composite $v_f = 55\%$	E_L 163545	E_T 9143	α_L 0.002	α_T 39.3	ν_L 0.24	ν_T –
Composite $v_f = 60\%$	E_L 178040	E_T 9672	α_L − 0.004	α_T 37.9	ν_L 0.24	ν_T –
Composite $v_f = 65\%$	E_L 192535	E_T 10241	α_L − 0.009	α_T 36.5	ν_L 0.24	ν_T –

Fig. 21. First prototype for measuring thermal curvature.

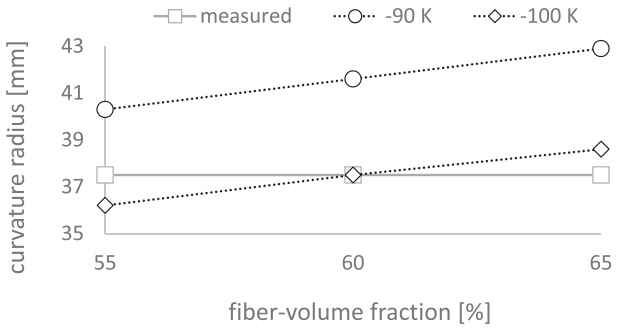

Fig. 22. Predicted curvature radii and measurement.

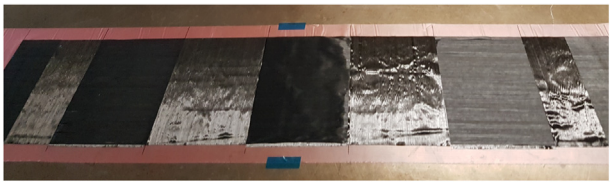

Fig. 23. Demonstrator laminate after laying process.

8.4. Corrugated-laminate demonstrator

Fig. 23 illustrates that the demonstrator laminate consists of nine regions,
$[90/0]_s - 3([0_2/90] - [90/0_2])) - [0_2/90] - [90/0]_s$, where the two outer regions on each side of the laminate have a width of 105 mm whereas all the inner regions have a width of 210 mm. Upon the curing process within the autoclave and removal of the auxiliary materials, the laminate takes on the shape of a corrugated laminate shown in Fig. 24.

9. Critical discussion

Handling of the corrugated-laminate demonstrator seen in Fig. 24 reveals that local bending stiffness is less than desirable. We suggest that this problem can be mitigated by using thermoplastic matrix materials with high processing or melting temperatures. Polyetheretherketon (PEEK) melts at $T_{melt} = 340$ °C. Its CTE of $\alpha = 47{\cdot}10^{-6}$ K^{-1} and tension modulus $E = 3600$ are comparable to the respective values seen in this study so that the use of PEEK, by virtue of a higher difference between consolidating and service temperatures, would increase the thickness-to-curvature radius by a factor of three if compared to the prototypes in this study, and consequently increase the

Fig. 24. Demonstrator laminate after laying process.

local bending stiffness by a factor of 27. The susceptibility to fatigue damage due to repeated morphing action remains a topic of further research.

10. Conclusion and outlook

This study has shown that mold-less forming of unsymmetric laminates solves the problem of manufacturing high-amplitude corrugated laminates. The nature of the forming mechanism dictates that the corrugation shape consist of piece-wise circular sections. The mathematical modeling has shown that combination of a 90° layer with two 0° layers give higher thermal curvatures than other numbers of 0° layers. Predictions of the mathematical model agree very well with FEM simulations. The said manufacturing process can be used to make corrugated laminates with integrated flat scales to produce an aerodynamically sufficiently smooth surface for application as flexible skin in morphing-wing design. Preliminary prototype and corrugated-laminate demonstrator validate the thermal-curvature predictions of the mathematical modeling. As tooling, other than necessary for making flat laminates, is not needed, the manufacturing method relying on thermal forming is more economic than other methods requiring molds or machinery.

Acknowledgment

The authors gratefully acknowledge the support of the Swiss National Science Foundation (project No. 169468 and Grant No. 200021_169468/1).

References

[1] Yokozeki T, Takeda S-I, Ogasawara T, Ishikawa T. Mechanical properties of corrugated composites for candidate materials of flexible wing structures. Compos Part A 2006;37(10):1578–86.
[2] Dayyani I, Shaw AD, Saavedra Flores E, Friswell M. The mechanics of composite corrugated structures: a review with applications in Morphing aircraft. Compos Struct 2015;133:358–80.
[3] Airoldi A, Sala G, Di Landro LA, Bettini P, Gilardelli A. Composite corrugated laminates for morphing applications. Concilio A, Lecce L, Dimino I, Pecora R, editors. Morphing wing technologies – large commercial aircraft and civil helicopters, 9. Milano, Italy: Elsevier, Politecnico di Milano; 2018,.. p. 247–76.
[4] Kress GR, Filipovic DT. An analytical nonlinear morphing model for corrugated laminates.
[5] Thurnherr C, Mirabito Y, Kress G, Ermanni P. Highly corrugated laminates deflection under uniform pressure. Compos Struct 2016;154:31–8.
[6] Thill C, Etches JA, Bond IP, Potter KD, Weaver PM, Wisnom MR. Investigation of trapezoidal corrugated aramid/epoxy laminates under large tensile displacements transverse to the corrugation direction. Compos Part A 2010;41(1):168–76. https://doi.org/10.1016/j.compositesa.2009.10.004.
[7] Xia Y, Ajaj RM, Friswell MI. The effects of corrugated skins on aerodynamic performances. J. Intell. Mater. Syst. Struct. 2014;25(7):786–94.
[8] Chavannas MA. Method of making an embossed laminated structure, US-3,026,231; 1962.
[9] Lemelson JH. Composite material, apparatus and methods for producing same, US-3,523,055; 1970.
[10] Johnson WR, Welsh RR. Sine wave beam web and method of manufacture, US-4,084,029; 1978.
[11] Donnecker PG, Varholak N, Jr., Schmitz MJ, Goodridge HM, Lauder JA, Skaggs KD. Method for fabricating a corrugated composite channel, US-5,882,462; 1999.
[12] Ashraf A. Method for producing a corrugated stretch laminate, US-7,501,034 B2; 2009.
[13] Thill C, Etches JA, Bond IP, Potter KD, Weaver PM. Corrugated composite structures for aircraft morphing skin applications. 18th International Conference of Adaptive Structures and Technologies. 2007. Ottawa, Ontario, Canada.
[14] Ghabezi P, Golzar M. Mechanical analysis of trapezoidal corrugated composite skins. Appl Compos Mater 2013;20(4):341–53. https://doi.org/10.1007/s10443-012-9267-6.
[15] Airoldi A, Fournier S, Borlandelli E, Bettini P, Sala G. Design and manufacturing of skins based on composite corrugated laminates for morphing aerodynamic surfaces. Smart Mater Struct 2013:1–12.
[16] Fournier S, Airoldi A, Borlandelli E, Sala G. Flexible composite supports for morphing skins. AIDAA Napoli XXII, Napoli, XXII Conference of Italien Association of Aeronautics and Astronautics, Naples, Italy. 2007.
[17] Thill C, Etches Ja, Bond IP, Potter KD, Weaver PM. Composite corrugated structures for morphing wing skin applications. Smart Mater Struct 2010;19(12):124009. https://doi.org/10.1088/0964-1726/19/12/124009.
[18] Panivalli P, Gilardelli A, Airoldi A, Quaranta G, Sala G. Morphing composite structures for adaptive high lift devices. In Proceedings of the 6th International Conference on Mechanics and Materials in Design, Ponta Delgada, Portugal. pp. 26–30.
[19] Schmitz A, Horst P. Bending deformation limits of corrugated unidirectionally reinforced composites. Compos Struct 2014;107:103–11.
[20] Fischer FJC, Beyrle M, Thellmann A-H, Endrass M, Stefani Th, Gerngross T, Kupke M. Corrugated composites: production-integrated quality assurance in carbon fiber reinforced thermoplastic sine wave beam production. Adv Manuf: Polym Compos Sci 2017;3(1):10–20.
[21] Kress G, Winkler M. Corrugated laminate homogenization model. Compos Struct 2010;92(3):795–810.
[22] Thurnherr C, Ruppen L, Kress G, Ermanni P. Interlaminar stresses in corrugated laminates. Compos Struct 2016;140:296–308.
[23] Khoo ZX, Teoh JEM, Liu Y, Chua CKC, Yang S, An J, et al. 3d printing of smart materials: a review on recent progresses in 4d printing. Virtual Phys Prototyping 2015;10(3):103–22.
[24] Hoa SV. Factors affecting the properties of composites made by 4d printing (moldless composites manufacturing). Adv Manuf: Polym Compos Sci 2017;3(3):101–9.
[25] Filipovic D, Kress G. A planar finite element formulation for corrugated laminates transverse shear force. Compos Struct 2018 available online.
[26] Jones RM. Mechanics of Composite Materials. New York: Hemisphere Publishing Corporation; 1975.
[27] Hyer MW. The room-temperature shapes of four-layer unsymmetric cross-ply laminates. J Compos Mater 1982;16:318.
[28] Kress GR, Filipovic DT. An analytical nonlinear morphing model for corrugated laminates. Curved Layered Struct 2019;6:56–66.
[29] Chamis CC. Simplified composite micromechanics equations for hygral, thermal, and mechanical properties. 38th Ann. Conf. of the Society of the Plastics Industry (SPI). Houston, TX; U.S.A.: Reinforced Plastics/Composites Inst.; 1983.